IV International Conference on Simulation for Additive Manufacturing
Sim-AM 2023
E. Rank and S. Kollmannsberger (Eds)

# CONTROLLING PHASE RATIO IN DIRECTED ENERGY DEPOSITION OF DUPLEX STAINLESS STEELS AND EFFECT ON STRESSES (SIM-AM 2023)

**D. WEISZ-PATRAULT**

École Polytechnique, Institut Polytechnique de Paris, LMS, CNRS, F-91128 Palaiseau, France
e-mail: daniel.weisz-patrault@cnrs.fr

**Key words:** Additive manufacturing, directed energy deposition, duplex steel, phase transformation, residual stress

**Abstract.** Optimal material properties of duplex stainless steels generally require near 50-50 ferrite-austenite microstructures. The development of additive manufacturing of duplex steels is hindered by difficulty in controlling cooling conditions to ensure a balanced phase ratio. In addition, non-uniform phase distribution is usually observed. Thus, sufficiently fast part-scale process simulations are interesting to optimize process parameters to better predict and control the temperature history during fabrication and therefore solid-state phase transitions. Furthermore, stresses should also be taken into account in the optimization of the phase field in order to avoid cracking, buckling or excessive distortions. Numerical results obtained from a fast modeling of directed energy deposition including thermal analysis, diffusion of alloying element to account for phase transitions, and stress computation are analyzed. On this basis, we investigate the effect on stresses of an optimized fabrication strategy designed to target uniform and balanced ferrite-austenite ratio with respect to a reference printing strategy.

## 1 INTRODUCTION

This paper focuses on directed energy deposition (DED) additive manufacturing (AM) of duplex stainless steel (DSS). Recently developed fast numerical simulation tools of DED enable to determine suitable process parameters and design additional temperature control devices to better control the ferrite-austenite phase ratio in super DSS parts that generally require near 50-50 ferrite-austenite microstructures [1]. In this paper, we consider grades such as super SAF 2507 DSS, which solidify as body-centered cubic (BCC) $\delta$-ferrite, which can transform into $\gamma$-austenite by diffusion of alloying elements. Controlling cooling rates in a specific temperature range is therefore essential to obtain balance phase ratio and overcome classical issues [2] that hinder the development of AM of DSS.

Since cooling conditions strongly depend on heat accumulation, distance to the substrate or local power and heat source speed variations, non-uniform phase distribution is usually observed in parts. Thus, to optimize process parameters and additional temperature control devices at the scale of the entire part, detailed local approaches focusing on the melt pool [3, 4, 5] are not suited. Instead, sufficiently fast part-scale process simulations [6, 7, 8, 9, 10] are necessary to optimize process parameters to better predict and control the temperature history during fabrication and therefore solid state phase transitions.

This paper presents numerical results relying on previously developed fast numerical approaches. (i) First we use a thermal analysis of DED [11, 12] based on analytical solutions, which can deal with relatively complex geometry, and takes account of latent heat release during solidification. This simulation of the temperature field history has already been validated experimentally by infrared measurements using pyrometers [11] and an infrared camera [13], and was used to predict grain growth [14, 15, 16] during thermal cycling. (ii) In addition, we use a fast model of diffusion of alloying elements based on analytical solutions to take into account phase transitions in DSS [17], which has recently been developed and coupled to [11] to predict ferrite-austenite phase ratio in thin-walled structures, with satisfying comparison against experimental measurements performed by electron backscatter diffraction techniques (EBSD). (iii) Furthermore, stresses also strongly depend on the complex temperature history, which should also be taken into account in the optimization of the phase field. In this contribution, we use a relatively fast mechanical model based on thick shell finite elements analysis (FEA) to predict mechanical response induced by thermal expansion and kinematic conditions between beads during fabrication [13].

## 2 NUMERICAL MODELS

General principles of the numerical models are briefly recalled here for the sake of clarity. The reader is refereed to [11, 17, 13] for details.

### 2.1 Thermal analysis

The fusion of the feedstock material is not considered, and liquid metal is directly deposited on the part at a temperature called deposition temperature denoted by $T_{\text{dep}}$ and determined for laser heat sources as a function of process parameters by using an analytical form [18, 11]. The computation of the temperature field also relies on the assumption that for single track multilayer structures, heat fluxes along the print direction are negligible in comparison to the build and transverse directions. Therefore, successive positions along the print direction are completely independent, which enables to reduce the 3D heat conduction problem to several 2D problems at different positions (called computation points) along the scanning path of the heat source. At each computation point, the heat conduction problem is decomposed into several simple multilayer heat conduction problems including heat convection with surrounding fluid and build platform as well as latent heat of fusion. Successive 2D multilayer problems are related to each other by setting the initial condition as the final condition of the previous problem and adding a new layer with $T_{\text{dep}}$ as initial temperature. This strategy enables to consider complex geometry and scanning strategy by considering the local radius of curvature for each computation point, and adjusting the times between successive metal depositions in order to correspond to the actual kinetics of the heat source. In addition, short computation time is ensured as each multilayer problem is solved analytically.

### 2.2 Diffusion assisted phase transition

Once the temperature field history is computed, one can consider solid-state phase transition. The $\delta \rightarrow \gamma$ phase transition is controlled by diffusion of alloying elements, and more specifically fast diffusion of N, and then slow diffusion of Cr and Ni (i.e., substitutionally-diffusing elements, which diffuse orders of magnitude slower than interstitial elements such as N). Only

Ni has been considered as Ni and Cr share similar diffusive properties. A two-species diffusion problem is therefore solved. First the phase transition is controlled by the fast diffusion of N between 1602-1587 K, and then the phase transition is controlled by slower diffusion of Ni for lower temperatures. Temperature ranges for which diffusion occurs have been computed using ThermoCalc. In addition, the $\delta \rightarrow \gamma$ phase transition arises by thickening of a continuous austenite layer formed at the ferrite grain boundaries (GB), and therefore depends on grain size. Therefore phase transition is modeled in a finite slab of size $R$ representing the grain size where the time dependent austenite thickness is defined by the moving $\delta/\gamma$ interface.

### 2.3 Stress computation

FEA adapted for AM often relies either on *element activation*, which consists in progressively adding new elements to the existing mesh, or *element penalization*, which consists in using a single global mesh whose stiffness is progressively switched from very low to realistic values as metal deposition goes on. The FEA developed in [13] combines both techniques as entire layers are progressively added to the domain, while at each time increment realistic stiffness is affected to a single element. Shell elements (i.e., 2D Reisner-Mindlin theory) are used as thin-walled structure is considered. Of course material properties not only depend on temperature but also on ferrite-austenite ratio and microstructure (e.g., grain size and morphology etc.). In this contribution though, average temperature dependent material properties are used as the main purpose is to capture the effect of different thermal regimes. Elastic and plastic average properties of SAF 2507 DSS are similar to 316L stainless steel reported in [19, 13], however the yield stress at room temperature of SAF 2507 DSS is around 600 MPa whereas it is only 350 MPa for 316L. The yield stress is modeled as an exponential law:

$$\sigma_Y(T) = \sigma_0 \left[1 + \beta_Y \, \exp\left(-\gamma_Y (T - T_0)\right)\right] \tag{1}$$

Where coefficients have been adjusted as follows: $\sigma_0 = 63.32$ MPa, $\beta_Y = 8.476$, and $\gamma_Y = 2.236 \times 10^{-3}$ K$^{-1}$. In addition, the thermal expansion coefficient is set to $\alpha = 14 \times 10^{-6}$ K$^{-1}$.

## 3 RESULTS AND DISCUSSION

In [17] several printing strategies using a DED machine have been proposed to produce thin-walled structures (50 mm long by 16 mm high) made of 100 layers. In this contribution, two of them are studied in more details: 1) the reference strategy in which the laser power is set to 250 W and the laser velocity is 2000 mm.min$^{-1}$ (see [17] for details), and 2) an optimized strategy, identical to the reference excepted that the substrate temperature is controlled during fabrication to obtain more balanced and uniform ferrite-austenite phase fraction. All process parameters, and thermal and diffusional properties of SAF 2507 DSS are listed in [17]. On this basis, thermo-mechanical computations are carried out in this contribution to estimate the mechanical effect of the optimized strategy with respect to the reference strategy.

In figure 1(left) the temperature kinetics during deposition of the fifth cycle are compared between the reference and the optimized printing strategies. As shown in figure 1(left) the $\delta \rightarrow \gamma$ transition is the most significant between 1600 and 1300 K, and it is clear that not only the temperature of the deposited layer (i.e., 5th) stays within this temperature range for a longer period for the optimized strategy than for the reference one, but some layers underneath also reach the transformation temperature range whereas only the deposited layer reaches it

for the reference one. Thermal cycling is therefore used to adjust the $\delta \rightarrow \gamma$ phase ratio in the optimized strategy. Resulting $\gamma$ phase fraction is presented in figure 1(right) in the thin-walled structure as a function of the distance from the substrate. The optimized strategy leads to more balanced and uniform phase ratio.

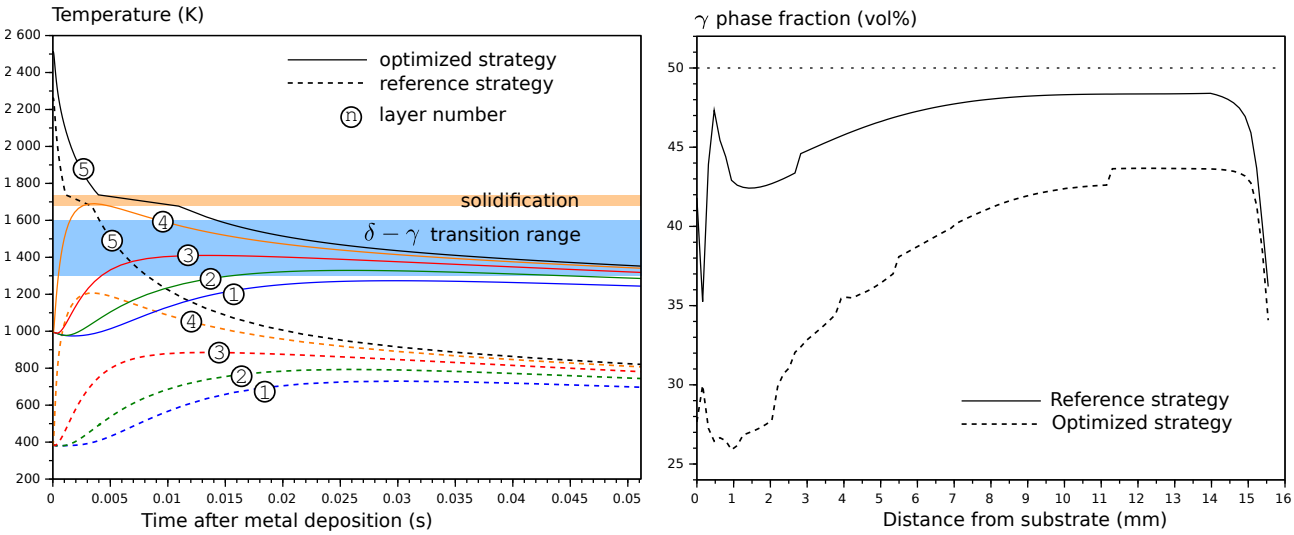


**Figure 1**: Temperature during deposition of the 5th layer for both reference and optimized printing strategies (left). Phase fraction in the thin-walled structure for both reference and optimized printing strategies(right).

Stress components at the end of the last layer of the optimized strategy is presented in figure 2(left) and a comparison with the reference computation is provided in figure 2(right). Non-negligible variations are observed. For instance, tension in the first few layers along the print direction is higher for the optimized strategy by around 20%, similarly tension along the build direction localized at the lower corners of the wall is higher for the optimized strategy by around 10%. Nevertheless such variations are confined to small regions of the wall and are not sufficient to compromise the fabrication.

## 4 CONCLUSION

The entire DED process of a 2507 duplex stainless steel has been simulated for 100 layers thin-walled structures according to different printing strategies. A reference strategy resulted in non-uniform and unbalanced phase ratio whereas an optimized printing strategy consisting in controlling the substrate temperature enabled to reach more balanced and uniform phase ratio. In addition, the analysis of stress components showed that tension increased non-negligibly in localized regions of the printed wall for the optimized strategy. Nevertheless, the overall stress field remains reasonable and does not compromise fabrication.

## REFERENCES

[1] J.-O. Nilsson, Super duplex stainless steels, Materials science and technology 8 (8) (1992) 685–700.

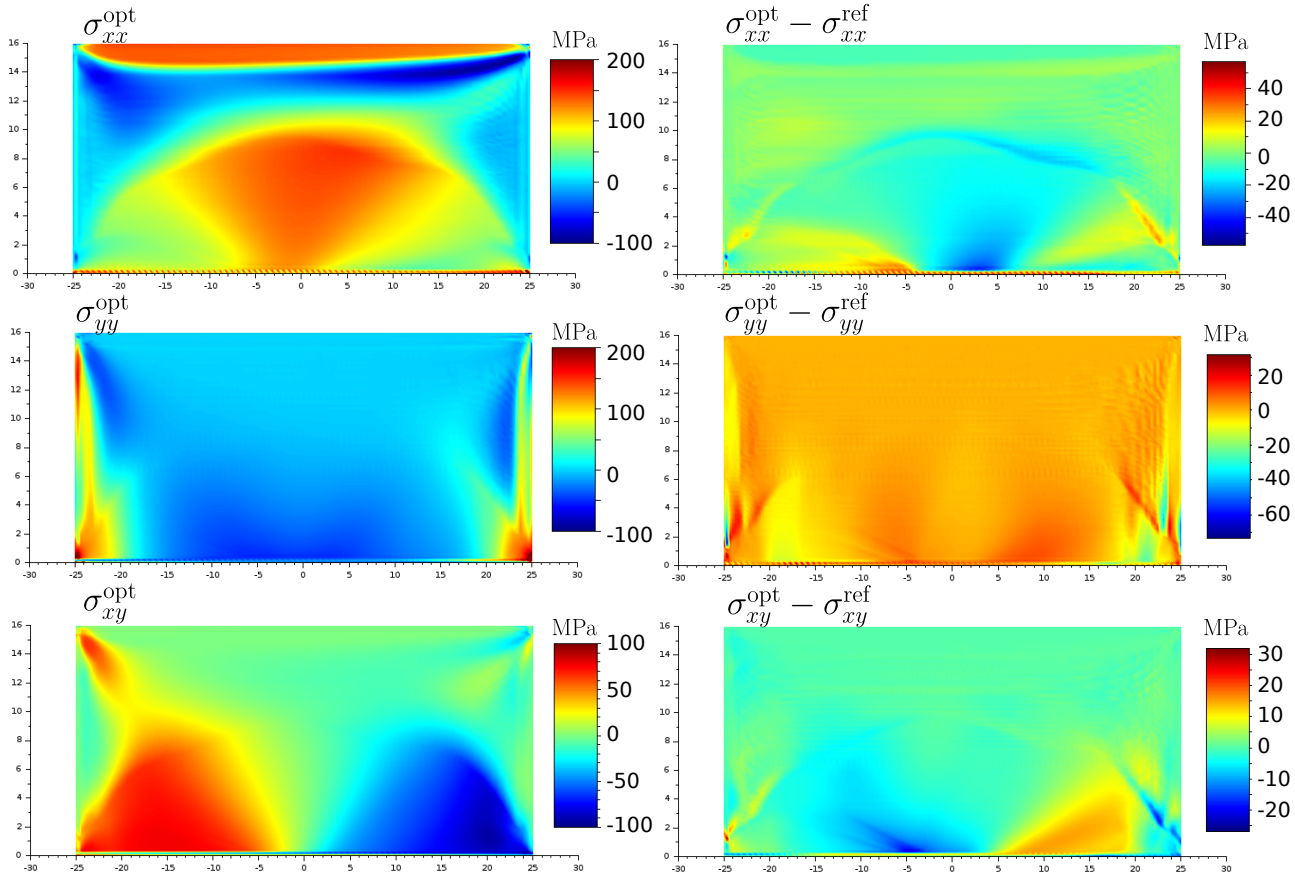


**Figure 2**: Stress components $\sigma_{xx}^{\mathrm{opt}}, \sigma_{yy}^{\mathrm{opt}}, \sigma_{xy}^{\mathrm{opt}}$ resulting from the optimized strategy, where $x, y$ are the print and build directions respectively (left). Difference between stress components resulting from the optimized and reference strategy $\sigma_{xx}^{\mathrm{opt}} - \sigma_{xx}^{\mathrm{ref}}, \sigma_{yy}^{\mathrm{opt}} - \sigma_{yy}^{\mathrm{ref}}, \sigma_{xy}^{\mathrm{opt}} - \sigma_{xy}^{\mathrm{ref}}$ (right).

[2] D. Zhang, A. Liu, B. Yin, P. Wen, Additive manufacturing of duplex stainless steels-a critical review, Journal of Manufacturing Processes 73 (2022) 496–517.

[3] Y. Lian, S. Lin, W. Yan, W. K. Liu, G. J. Wagner, A parallelized three-dimensional cellular automaton model for grain growth during additive manufacturing, Computational Mechanics 61 (5) (2018) 543–558.

[4] H. Wei, G. Knapp, T. Mukherjee, T. DebRoy, Three-dimensional grain growth during multi-layer printing of a nickel-based alloy inconel 718, Additive Manufacturing 25 (2019) 448–459.

[5] C. Kumara, A. Segerstark, F. Hanning, N. Dixit, S. Joshi, J. Moverare, P. Nylén, Microstructure modelling of laser metal powder directed energy deposition of alloy 718, Additive Manufacturing 25 (2019) 357–364.

[6] J. Smith, W. Xiong, J. Cao, W. K. Liu, Thermodynamically consistent microstructure prediction of additively manufactured materials, Computational mechanics 57 (3) (2016) 359–370.

[7] D. Zhang, Z. Feng, C. Wang, Z. Liu, D. Dong, Y. Zhou, R. Wu, Modeling of temperature field evolution during multilayered direct laser metal deposition, Journal of Thermal Spray Technology 26 (5) (2017) 831–845.

[8] C. Baykasoglu, O. Akyildiz, D. Candemir, Q. Yang, A. C. To, Predicting microstructure evolution during directed energy deposition additive manufacturing of ti-6al-4v, Journal of Manufacturing Science and Engineering 140 (5) (2018) 051003.

[9] J. Li, Q. Wang, P. P. Michaleris, An analytical computation of temperature field evolved in directed energy deposition, Journal of Manufacturing Science and Engineering 140 (10) (2018) 101004.

[10] C. Guévenoux, M. Nasiry, S. Durbecq, A. Charles, E. Charkaluk, A. Constantinescu, Thermal modeling of ded repair process for slender panels by a 2d semi-analytic approach (2020).

[11] D. Weisz-Patrault, Fast simulation of temperature and phase transitions in directed energy deposition additive manufacturing, Additive Manufacturing 31 (2020) 100990.

[12] D. Weisz-Patrault, Fast macroscopic thermal analysis for laser metal deposition. Application to multiphase steels, in: Sim-AM 2019: II International Conference on Simulation for Additive Manufacturing, CIMNE, 2019, pp. 60–71.

[13] D. Weisz-Patrault, P. Margerit, A. Constantinescu, Residual stresses in thin walled-structures manufactured by directed energy deposition: In-situ measurements, fast thermo-mechanical simulation and buckling, Additive Manufacturing (2022) 102903.

[14] D. Weisz-Patrault, S. Sakout, A. Ehrlacher, Fast simulation of temperature and grain growth in directed energy depostion additive manufacturing, in: 14th World Congress on Computational Mechanics, Vol. 1, ECCOMAS Congress, 2020, p. 2748.

[15] S. Sakout, D. Weisz-Patrault, A. Ehrlacher, Energetic upscaling strategy for grain growth. I: Fast mesoscopic model based on dissipation, Acta Materialia 196 (2020) 261–279.

[16] D. Weisz-Patrault, S. Sakout, A. Ehrlacher, Energetic upscaling strategy for grain growth. II: Probabilistic macroscopic model identified by Bayesian techniques, Acta Materialia (2021).

[17] A. Edwards, D. Weisz-Patrault, E. Charkaluk, Analysis and fast modelling of microstructures in duplex stainless steel formed by directed energy deposition additive manufacturing, Additive Manufacturing 61 (2023) 103300.

[18] D. Bäuerle, Laser processing and chemistry, Springer Science & Business Media, 2013.

[19] P. Margerit, D. Weisz-Patrault, K. Ravi-Chandar, A. Constantinescu, Tensile and ductile fracture properties of as-printed 316l stainless steel thin walls obtained by directed energy deposition, Additive Manufacturing 37 (2021) 101664.